$Rb_2BaNb_2Se_{11}$: A new quaternary niobium polyselenide with infinite anionic chains composed of Nb_2Se_{11} building block

Yuandong Wu, Christian Näther, Wolfgang Bensch*

Institut für Anorganische Chemie, Christian-Albrechts-Universität zu Kiel, Olshausenstr. 40, D-24108 Kiel, Germany

Abstract

The quaternary compound $Rb_2BaNb_2Se_{11}$ has been synthesized by reacting Nb metal with an in situ formed flux of Rb_2Se_3, BaSe and Se at 773 K. $Rb_2BaNb_2Se_{11}$ crystallizes in the monoclinic space group $P2_1/c$ with four formula units and lattice parameters $a = 7.8438(5)$ Å, $b = 13.6959(6)$ Å, $c = 17.0677(13)$ Å, $\beta = 97.917(9)°$. The structure consists of one-dimensional anionic chains formed by interconnection of dimeric $[Nb_2Se_{11}]$ units. The chains are directed along the crystallographic c-axis with Rb^+ and Ba^{2+} ions being located between the chains. The $[Nb_2Se_{11}]$ units are formed by face sharing of two $NbSe_7$ bipyramids and are joined by Se_2^{2-} dianions to form infinite $^1_\infty[Nb_2Se_{11}^{4-}]$ chains. The compound was characterized with infrared spectroscopy in the FIR region, Raman and UV/Vis diffuse reflectance spectroscopy.

© 2006 Elsevier Inc. All rights reserved.

Keywords: Quaternary niobium selenide; Molten flux method; Crystal structure; IR; Raman spectroscopy

1. Introduction

Low-dimensional solid-state compounds are of interest due to their structural and different interesting physical properties such as superconductivity, the formation of charge density waves, and low-dimensional magnetism. Since the first report about the synthesis of a polychalcogenide in an alkali chalcogenide flux at medium temperatures (250–500 °C) [1], a remarkable variety of low-dimensional multinary transition metal polychalcogenides have been synthesized [2,3]. Among these compounds polychalcogenides of Nb and Ta containing infinite chains form an interesting group [4]. Representative examples are $NaNbS_6$ [5], $KTaS_5$ [6], $A_4Nb_2Se_{11}O$ ($A = K$, Cs) [7], $Rb_{12}Nb_6Se_{35}$ [8], $K_{12}Ta_6Se_{35}$ [9], $K_3CuNb_2Se_{12}$ [10] and $Rb_3AgTa_2Se_{12}$ [11]. Both, $NaNbS_6$ and $KTaS_5$ are two exceptions in the large family of ternary Nb/Ta polysulfides. Most ternary polysulfides contain pure and expanded M_2S_{11} ($M = Nb$, Ta) groups, in which two pentagonal MS_7 bipyramids share a common face, whereas the structures of $NaNbS_6$ and $KTaS_5$ are composed of one-dimensional chains that are connected via face-sharing of NbS_9 polyhedra and edge-sharing of TaS_8 polyhedra, respectively. In contrast to polysulfides, all polyselenides mentioned above contain M_2Se_{11} ($M = Nb$, Ta) building blocks that are linked by different Se_n^{2-} anions or via MSe_4 ($M = Cu$, Ag) tetrahedra to form one-dimensional chains. Compared to polysulfides, the number of polyselenides reported is rather low. Until now all polysulfides and polyselenides were prepared with alkali and/or coinage metals. Very recently we reported the syntheses and characterization of the first alkaline-earth metal containing Nb compounds with compositions $KBaNbS_4$ [12] and $K_4Ba_2(Nb_2S_{11})_2$ [13].

In our continuing synthetic work, we successfully prepared the hitherto unknown polyselenide $Rb_2BaNb_2Se_{11}$. In the paper we report the synthesis, crystal structure and characterization of this new quaternary polyselenide, exhibiting a new binding mode within the Nb_2Se_{11} building blocks and an interconnection scheme between these units which was never observed before.

---

*Corresponding author. Fax: +49 431 880 1520.

E-mail address: wbensch@ac.uni-kiel.de (W. Bensch).

2. Experimental

2.1. Reagents

The following reagents were used as obtained unless especially noted: (i) Rb metal, 99.0%, ABCR GmbH & Co. KG; (ii) BaSe, 99.5%, Alfa Aesar; (iii) Nb powder, 99.8%, 325 mesh, Alfa Aesar; (iv) Ta powder, 99.98%, 325 mesh, ABCR GmbH & Co.KG; (v) Se powder, 99.5%, 200 mesh, Retorte Ulrich Scharrer GmbH.

2.2. Synthesis

Rb_2Se_3 was prepared from the reaction of stoichiometric amounts of elemental Rb and Se powder in liquid ammonia under an argon atmosphere.

$Rb_2BaNb_2Se_{11}$: Rb_2Se_3, BaSe, Nb, and Se in a 2/1/2/8 mmolar ratio, were thoroughly mixed in a nitrogen filled glove box. The mixture was then loaded into a glass ampoule (Duran®) which was subsequently evacuated ($\sim 2 \times 10^{-3}$ mbar) and flame sealed. The ampoule was heated from 25 to 500 °C in 24 h and kept at this temperature for 6 days, cooled to 100 °C at a rate of 2 °C/h followed by cooling to room temperature in 4 h. The resulting black melt was washed with DMF and acetone and the product was dried in vacuum. The product consists of black platelet crystals ($\sim$40%) together with transparent dark red platelet crystals. The crystals are stable in dry air for a long time, but decompose slowly under humid conditions. Single crystals were selected for elemental analysis, X-ray diffraction and optical properties measurements.

2.3. Elemental analysis

Selected crystals were analyzed by energy dispersive X-ray spectroscopy (EDX) performed on Philips ESEM XL 30 SEM equipped with an EDAX detector. EDX data indicated that the red platelet crystals were $BaSe_3$ [14], while the black platelet crystals gave an average composition $Rb_2BaNb_{1.9}Se_{10.7}$, which is in good agreement with the result from single crystal structure determination.

2.4. X-ray crystallography

A black platelet crystal with dimensions of $0.13 \times 0.10 \times 0.05$ mm³ was manually selected from the reaction product and mounted on top of a glass fiber and bathed in a cold nitrogen stream at -73 °C. A STOE Imaging Plate Diffraction System (IPDS-1) with graphite monochromatized MoKα radiation was used for data collection. The raw intensities were treated in the usual way applying a Lorentz, polarization and numerical absorption correction. The structure was solved using direct methods and refined using the SHELXTL [15] package of crystallographic programs. The systematic absences clearly pointed to the space group $P2_1/c$ with all atoms being

located in general positions. All atoms were subsequently refined with anisotropic thermal displacement parameters yielding the final R_1 and wR_2 values of 0.0358 and 0.0948, respectively. Technical details of the data acquisition as well as some refinement results are summarized in Table 1. Atomic coordinates and equivalent isotropic displacement parameters are given in Table 2. Selected bond distances are listed in Table 3.

Further details of the crystal structure investigation can be obtained from the Fachinformationszentrum Karlsruhe, 76344 Eggenstein-Leopoldshafen, Germany (fax: +49 7247 808 666; E-mail: crysdata@fiz-karlsruhe.de), on quoting the depository number CSD-416574.

2.5. Physical measurements

Infrared spectroscopy. MIR spectra were recorded on a Genesis FT-Spectrometer (ATI Mattson) in the range between 400 and 4000 cm^{-1}. Resolution was 2 cm^{-1} and $Rb_2BaNb_2Se_{11}$ was prepared as a KBr pellet. Far-IR spectra were collected between 80 and 550 cm^{-1} (resolution

Table 1
Technical details of data acquisition and some refinement results for $Rb_2BaNb_2Se_{11}$

Empirical formula	$Rb_2BaNb_2Se_{11}$
Formula weight/g/mol	1362.66
Temperature	200 K
Wavelength/Å	0.71073
Crystal system	Monoclinic
Space group	$P2_1/c$
a/Å	7.8438(5)
b/Å	13.6959(6)
c/Å	17.0677(13)
β/deg.	97.917(9)
V/Å³	1816.1(2)
Z	4
Calculated density/g cm^{-3}	4.984
Crystal color	Black
μ/mm^{-1}	30.73
$F(000)$	2344
Crystal size/mm³	$0.13 \times 0.10 \times 0.05$
θ range	2.41–8.07°
Index range	$-10 \leqslant h \leqslant 10$
	$-18 \leqslant k \leqslant 18$
	$-22 \leqslant l \leqslant 22$
Reflections collected	19044
Independent reflections	4385
R_{int}	0.0888
Completeness to $\theta = 28.07°$	99.2%
Refinement method	Full-matrix least square on F^2
Min./max. transm.	0.0125/0.0881
Refl. with $F_o > 4\sigma(F_o)$	3854
Number of parameters	146
Goodness-of-fit on F^2	1.013
Final R indices $(F_o > 4\sigma(F_o))$[a,b]	$R_1 = 0.0358$, $wR_2 = 0.0912$
R indices (all data)[a,b]	$R_1 = 0.0427$, $wR_2 = 0.0948$
Extinction coefficient	0.00094(9)
Largest diff. peak and hole/eÅ^{-3}	3.000/-2.068

[a] $R_1 = \sum||F_o| - |F_c||/\sum|F_o|$.
[b] $wR_2 = [\sum w(F_o^2 - F_c^2)^2/\sum w(F_o^2)^2]^{1/2}$, $w = 1/[\sum(F_o^2) + (aP)^2 + bP]$, where $P = (\max(F_o^2, 0) + 2F_c^2)/3$.

Table 2
Atomic coordinates and equivalent isotropic displacement parameters U_{eq} ($\text{Å}^2 \cdot 10^3$) for $Rb_2BaNb_2Se_{11}$

	x	y	z	U_{eq}
Nb(1)	0.1459(1)	0.3274(1)	0.8059(1)	7(1)
Nb(2)	0.2788(1)	0.2834(1)	0.6076(1)	6(1)
Se(1)	0.2090(1)	0.4484(1)	0.9004(1)	19(1)
Se(2)	0.0418(1)	0.7164(1)	0.6132(1)	10(1)
Se(3)	0.3902(1)	0.2959(1)	0.3506(1)	14(1)
Se(4)	0.5530(1)	0.6754(1)	0.2452(1)	10(1)
Se(5)	0.1623(1)	0.6364(1)	0.2668(1)	11(1)
Se(6)	−0.0729(1)	0.4723(1)	0.3249(1)	8(1)
Se(7)	0.1450(1)	0.1583(1)	0.6984(1)	10(1)
Se(8)	−0.0040(1)	0.8161(1)	0.4327(1)	10(1)
Se(9)	0.5910(1)	0.5428(1)	0.3894(1)	10(1)
Se(10)	0.1590(1)	0.3790(1)	0.4770(1)	9(1)
Se(11)	0.5114(1)	0.8127(1)	0.4435(1)	13(1)
Ba(1)	0.2594(1)	0.6224(1)	0.4717(1)	14(1)
Rb(1)	0.2973(1)	0.8844(1)	0.2669(1)	14(1)
Rb(2)	−0.2682(1)	0.0457(1)	0.4145(1)	25(1)

Estimated standards deviations are given in parentheses. The U_{eq} is defined as one third of the trace of the orthogonalized U_{ij} tensor.

Table 3
Selected bond distances (Å) for $Rb_2BaNb_2Se_{11}$. Estimated standards deviations are given in parentheses

Nb(1)–Se(1)	2.3173(10)	Nb(1)–Se(3)	2.5886(10)
Nb(1)–Se(5)	2.6079(10)	Nb(1)–Se(6)	2.6157(9)
Nb(1)–Se(4)	2.6277(10)	Nb(1)–Se(2)	2.6456(10)
Nb(1)–Se(7)	2.9539(9)	Nb(2)–Se(11)	2.3656(10)
Nb(2)–Se(8)	2.5631(10)	Nb(2)–Se(9)	2.5872(9)
Nb(2)–Se(7)	2.6247(9)	Nb(2)–Se(10)	2.6435(9)
Nb(2)–Se(4)	2.7319(10)	Nb(2)–Se(6)	2.8899(9)
Se(2)–Se(10)	2.4175(10)	Se(3)–Se(4)	2.4065(11)
Se(5)–Se(6)	2.3798(10)	Se(7)–Se(8)	2.3813(10)
Ba(1)–Se(9)	3.3065(9)	Ba(1)–Se(11)	3.3454(9)
Ba(1)–Se(9)	3.3697(9)	Ba(1)–Se(8)	3.3726(9)
Ba(1)–Se(2)	3.3852(9)	Ba(1)–Se(6)	3.4261(9)
Ba(1)–Se(10)	3.4293(9)	Ba(1)–Se(5)	3.4805(9)
Ba(1)–Se(10)	3.5120(9)	Rb(1)–Se(1)	3.3695(11)
Rb(1)–Se(6)	3.3794(10)	Rb(1)–Se(2)	3.3807(11)
Rb(1)–Se(11)	3.3872(11)	Rb(1)–Se(4)	3.5437(10)
Rb(1)–Se(5)	3.5572(11)	Rb(1)–Se(3)	3.5844(11)
Rb(1)–Se(9)	3.6374(11)	Rb(1)–Se(7)	3.6463(11)
Rb(2)–Se(1)	3.4029(12)	Rb(2)–Se(5)	3.5362(12)
Rb(2)–Se(7)	3.6007(11)	Rb(2)–Se(8)	3.6615(12)
Rb(2)–Se(11)	3.6962(12)	Rb(2)–Se(4)	3.7266(12)
Rb(2)–Se(8)	3.7550(12)	Rb(2)–Se(2)	3.7685(11)
Rb(2)–Se(1)	3.7843(13)	Rb(2)–Se(11)	3.8149(12)

2 cm^{-1}) on an ISF-66 device (Bruker) with the sample pressed in polyethylene pellet.

Raman spectroscopy. Raman spectra were collected on an ISF-66 spectrometer (Bruker) with additional FRA 106 Raman module. A Nd/YAG laser was used as source of excitation ($\lambda = 1064$ nm). The samples were ground and prepared on Al sample holders. The measuring range was −1000 to 3500 cm^{-1} with a resolution of 2 cm^{-1}.

Solid-state UV/Vis/NIR spectroscopy: UV/vis/NIR diffuse reflectance spectra were recorded on a Cary 5 spectrometer (Varian Techtron Pty.). The spectrometer was equipped with an Ulbricht sphere (Diffuse reflectance accessory; Varian Techtron Pty.). The inner wall of the Ulbricht sphere (diameter) 110 mm was covered with a PTFE layer of 4 mm thickness. A PbS detector (NIR) and a photomultiplier (UV/vis) were attached to the Ulbricht sphere.

The sample was ground together with BaSO$_4$ and prepared as a flat specimen. Resolution was 1 nm for the UV/vis range and 2 nm for the near-IR range. The measuring range was 250–2000 nm. BaSO$_4$ was used as standard for 100% reflectance. Absorption data were calculated from the reflectance data using the Kubelka–Munk function [16]. The approximate band gap was determined as the intersection point between the energy axis and the line extrapolated from the linear part of the absorption edge in a $(F(R))^2$ versus energy plot.

3. Results and discussion

3.1. Crystal structure

The new quaternary niobium polyselenide $Rb_2BaNb_2Se_{11}$ crystallizes in the monoclinic space group $P2_1/c$ with one crystallographically independent Ba, two unique Rb and Nb as well as eleven unique Se atoms that are located on general positions. In the crystal structure the $^1_\infty[Nb_2Se_{11}]^{4-}$ anionic chains running along the c-axis are well-separated by the Rb and Ba cations (Fig. 1).

The shortest inter-chain Se–Se distance of 3.751(2) Å is slightly shorter than the sum of the van der Waals radii (3.8 Å). Every chain is surrounded by six other chains in a pseudo-hexagonal fashion (Fig. 1). Each of the two crystallographically independent Nb atoms is seven co-ordinated and resides in a distorted pentagonal bi-pyramid of Se atoms (Fig. 2). Nb(1) is coordinated by one terminal Se^{2-}, two η^2-Se$_2^{2-}$ anions and one η^1-Se$_2^{2-}$ anion which both are linked to Nb(2), and an additional Se atom of a Se$_2^{2-}$ unit which is connected to the Nb(2) atom in the next Nb$_2$Se$_{11}$ group. In contrast, Nb(2) has bonds to two Se^{2-} anions, one η^2-Se$_2^{2-}$ anion, two η^1-Se$_2^{2-}$ anions which are bound to Nb(1), and an additional Se atom of Se$_2^{2-}$ which is connected to a Nb(1) atom in another Nb$_2$Se$_{11}$ unit. The coordination mode of the $^1_\infty[Nb_2Se_{11}]^{4-}$ anionic chain can be described as $[Nb_2(\mu_2\text{-}\eta^2,\eta^1\text{-Se}_2)_3(Se)_3(\mu_2\text{-}\eta^1,\eta^1\text{-Se}_2)]^{4-}$ and the assignment of the formal valences are Rb$^+$, Ba^{2+}, Nb^{5+}, Se$_2^{2-}$ and Se^{2-}. We note that the connection modes in Tl$_4$Ta$_2$Se$_{11}$ [17] and K$_6$Nb$_4$Se$_{22}$ [18] are quite different and may be described as $[Ta_2(\mu\text{-Se})(\mu\text{-}\eta^2,\eta^1\text{-Se}_2)_2(\eta\eta^2\text{-Se}_2)_2(Se)_2]^{4-}$ and $[Nb_2(\mu\text{-}\eta^2,\eta^1\text{-Se}_2)_3(\eta^2\text{-Se}_2)(Se)_2]_2(\mu\text{-}\eta^1\text{-Se}_2)]^{6-}$, respectively. Comparing the structures of the above-mentioned two compounds with that of $Rb_2BaNb_2Se_{11}$ a close relationship with the structure of K$_6$Nb$_4$Se$_{22}$ [18] is obvious. The conformations of Nb$_2$Se$_{11}$ units in both compounds are almost identical. The
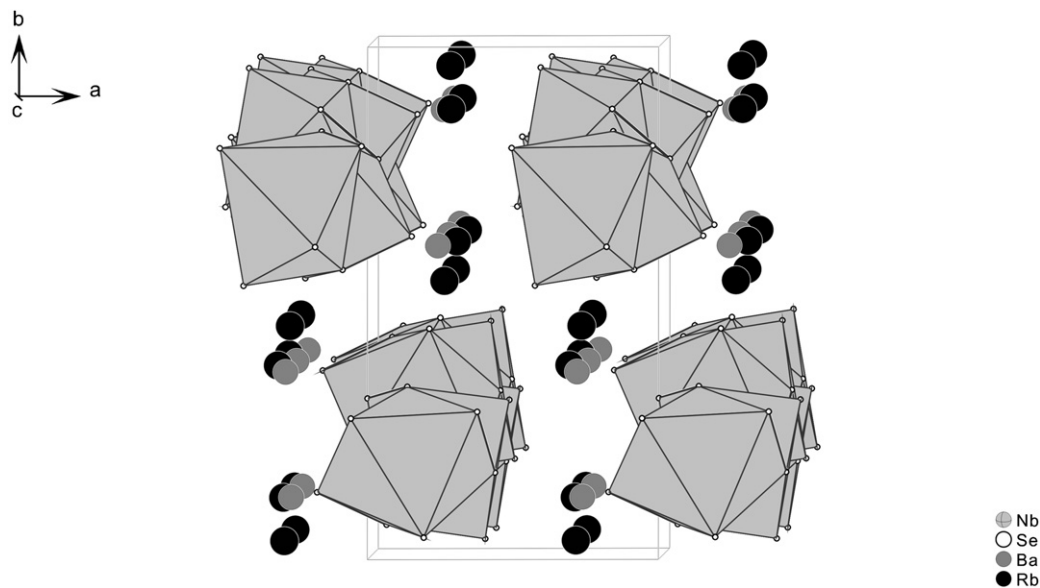
Fig. 1. View of crystal structure of $Rb_2BaNb_2Se_{11}$ with infinite $^1_\infty[Nb_2Se_{11}]^{4-}$ chains along [0 0 1]. The $[Nb_2Se_{11}]$ units are represented as polyhedra.

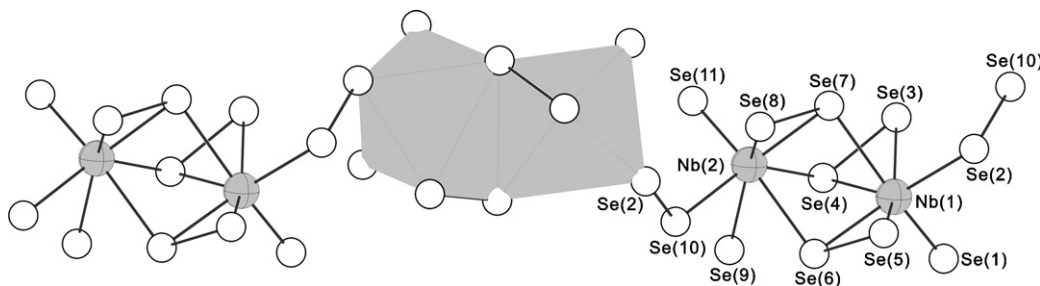

Fig. 2. Interconnection of the $[Nb_2Se_{11}]$ units into chains with atomic labeling. One $[Nb_2Se_{11}]$ unit is emphasized as polyhedron for clarity.

structure of the anionic chains in $Rb_2BaNb_2Se_{11}$ can be derived by cleavage of the Se–Se bonds of two η^2-Se_2 groups in the Nb_4Se_{22} units in $K_6Nb_4Se_{22}$. One Se atom of each Se_2 group forms a bond to a Se atom of neighbored Nb_4Se_{22} units yielding the infinite chains, whereas the second Se atom remains terminal (Se(9) in $K_2BaNb_2Se_{11}$). A comparison between $Rb_{12}Nb_6Se_{35}$ [8] and $Rb_2BaNb_2Se_{11}$ shows that the connection mode in the former compound is completely different ($[(Nb_2(\mu$-η^2,η^2-$Se_3)(\mu$-η^2,η^1-$Se_2)_2(Se_2)_2(Se)_2)_3$ $(\mu$-η^1-$Se_3)_2(\mu$-η^1-$Se_2)]^{12-}$) containing μ-η^2,η^2-Se_3 and μ-η^1-Se_3 groups which do not exist in $Rb_2BaNb_2Se_{11}$.

Each Nb atom has a short bond to an axial Se^{2-} anion (Nb(1)–Se(1): 2.3173(10) Å and Nb(2)–Se(11): 2.3656(10) Å). Ten medium long Nb–Se distances are between 2.5631(10) and 2.7319(10) Å, and two longer distances (2.8899(9) and 2.9539(9) Å) are observed to the Se atoms of η^2-Se_2^{2-} anions attached to the neighboring Nb atom. The long bonds are in trans position to the short Nb–Se bonds (Table 3). The average distance of 2.63 Å is in agreement with the sum of the ionic radii (Nb^{5+}: 0.69 Å; Se^{2-}: 1.98 Å) [19], and it also matches with the average Nb–Se distance of 2.62 and 2.67 Å reported for $K_4Nb_2Se_{11}O$ and $Cs_4Nb_2Se_{11}O$ [7]. A careful inspection of Nb–Se bonds to

terminal Se atoms shows that the Nb(2)–Se(9) bond length (2.5872(9) Å) is much longer than Nb(1)–Se(1) (2.3173(10) Å) and Nb(2)–Se(11) (2.3656(10) Å). A possible reason for the elongation may be weak interactions between Se(9) and Se(4), Se(6), and Se(10) with distances Se(9)–Se(4) (3.0399(2) Å), Se(9)–Se(6) (3.0203(2) Å), and Se(9)–Se(10) (2.9939(3) Å), all being remarkably shorter than the sum of the van der Waals radii of two Se atoms and longer than a Se–Se single bond. As expected the environment of the Se anions is different in the title compound compared with that found in $K_6Nb_4Se_{22}$ [18]. The Se(9) atom in $Rb_2BaNb_2Se_{11}$ is surrounded by one Rb^+ ion and two Ba^{2+} ions with the distances of 3.6374(11) (Se(9)–Rb(1), 3.3065(9) and 3.3697(9) Å (Se(9)–Ba(1)), and the corresponding Se atom in $K_6Nb_4Se_{22}$ is coordinated by four K^+ ions. The Nb_2Se_{11} unit in $Rb_2BaNb_2Se_{11}$ is surrounded by six Rb^+ ions and three Ba^{2+} ions which are located near the Nb(1)Se_7 polyhedron. To demonstrate the differences between the structures the volumes of the $NbSe_7$ polyhedra were calculated using the program VOLCAL in the WinGX package [24]. The volume of 26.59(1) Å^3 for Nb(1)Se_7 polyhedron in $Rb_2BaNb_2Se_{11}$ is almost identical with those

for Nb(1)Se$_7$ (26.73(2) Å^3 in K$_4$Nb$_2$Se$_{11}$O [7] and 26.50(1) in Rb$_{12}$Nb$_6$Se$_{35}$ [8]), whereas the volume for Nb(2)Se$_7$ of 27.09(1) Å^3 in Rb$_2$BaNb$_2$Se$_{11}$ is slightly larger. These results suggest that Nb$_2$Se$_{11}$ units tolerate some volume variation with different bonding of Se atoms and the connection modes of Nb$_2$Se$_{11}$ units.

The Nb–Nb separation of 3.7247(3) Å is significantly longer than in metallic Nb (2.858 Å), indicative for no significant Nb–Nb interaction. The Se–Se bonds in the Se$_2^{2-}$ anions are between 2.3798(10) and 2.4175(10) Å (average: 2.3963 Å), typical for Se–Se single bonds. The mean displacement of the Nb^{5+} ions from the least squares planes defined by Se(2)–Se(3)–Se(4)–Se(5)–Se(6) and Se(4)–Se(7)–Se(8)–Se(9)–Se(10) amounts to 0.49 Å for Nb(1) and 0.51 Å for Nb(2). The angle between the two "pentagonal planes" of 53.7° is significantly larger than that of 26.4° in the Ta$_2$Se$_{11}$ unit of Tl$_4$Ta$_2$Se$_{11}$ [17].

With a cut-off of about 4.0 Å for Rb–Se and Ba–Se distances the coordination numbers for Rb$^+$ and Ba^{2+} cations are 9 (Rb(1)) and 10 (Rb(2), Ba(1)), with distances ranging from 3.3695(11) to 3.8149(12) Å for Rb$^+$ cations and 3.3065(9) to 3.9649(9) Å for Ba^{2+}. The average distances are 3.50, 3.67, and 3.47 Å for Rb(1)–Se, Rb(2)–Se, and Ba(1)–Se, respectively. The mean Rb(2)–Se distance corresponds well with the sum of ionic radii (Rb$^+$, 1.66 Å (CN = 10); Se^{2-}: 1.98 Å), while the mean values for Rb(1)–Se and Ba(1)–Se are about 4% shorter than the sum of ionic radii (Rb$^+$: 1.63 Å (CN = 9); Ba^{2+}: 1.52 Å (CN = 10)) [19].

3.2. Optical properties

The far-IR and FT-Raman spectra of Rb$_2$BaNb$_2$Se$_{11}$ in the range 80–400 cm^{-1} are shown in Figs. 3 and 4. The FIR spectrum displays absorptions at 331, 311, 287, 242, 228, 177, 156, 120, 111, and 94 cm^{-1}, and the Raman spectrum shows shifts at 333, 321, 309, 290, 266, 232, 187, 178, 157, 122, 110, and 98 cm^{-1}. The modes at 242 and 228 cm^{-1} in
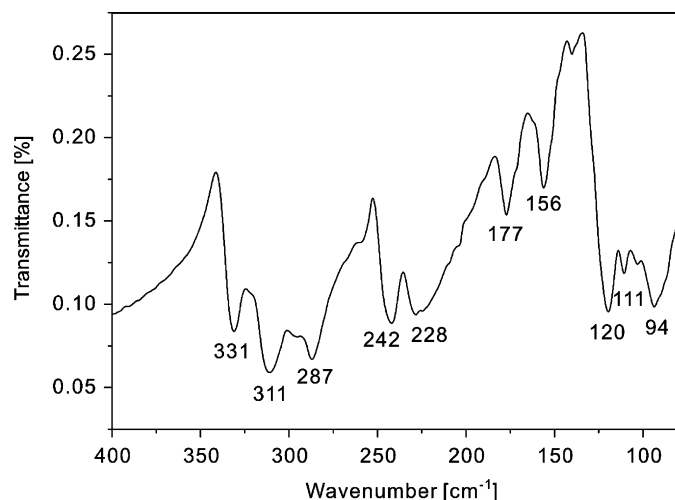

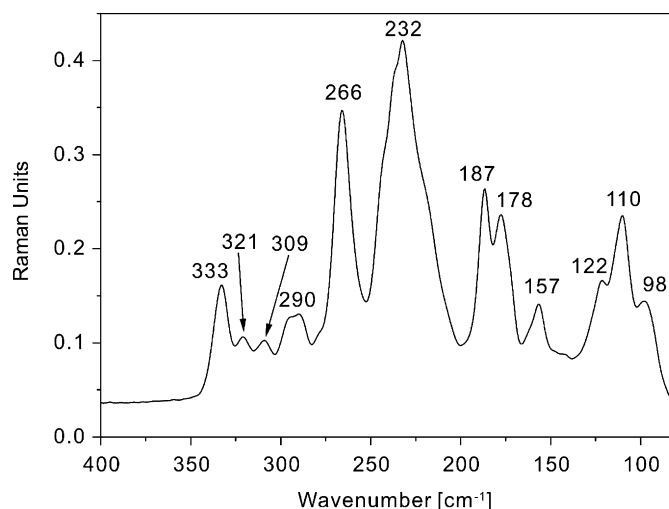
Fig. 4. FT-Raman spectrum of Rb$_2$BaNb$_2$Se$_{11}$.

the FIR and the bands at 266 and 232 cm^{-1} in the Raman spectrum can be assigned to Se–Se stretching vibrations. The wave number at which the stretching vibrations of a normal Se–Se bond occurs is variable and depends upon the local geometry of the Se atoms as well as the metal atom being bound to Se. For example, in (NbSe$_4$)$_3$I the stretching vibration appears at 278 cm^{-1} [20], for Rb$_2$Se$_2$ the values are 266 and 250 cm^{-1} [21], and in (Se$_2$SN$_2$)$_2$Cl$_2$ it is observed at 269 cm^{-1} [22]. The absorptions at 120, 111, and 94 cm^{-1} in the IR spectrum and the resonances at 122, 110, and 98 cm^{-1} in the Raman spectrum may be a result of deformation modes of Se–Nb–Se, judging from the Se–Nb–Se deformation frequencies reported for other compounds such as Tl$_3$NbSe$_4$ and Cu$_3$TaSe$_4$ [23]. However, it is difficult to unequivocally assign the shifts to distinct Nb–Se vibrations. According to the data published for Tl$_4$Ta$_2$Se$_{11}$ [17], the remaining signals may be mainly due to Nb–Se stretching modes.

The solid-state diffuse reflectance UV/vis spectrum of Rb$_2$BaNb$_2$Se$_{11}$ reveals a steep absorption edge corresponding to a band gap of 1.53 eV which is consistent with the black color. Compared with for instance Rb$_{12}$Nb$_6$Se$_{35}$ [8], the introduction of Ba^{2+} in the structure increases the band gap by about 0.13 eV.

4. Conclusions

The new polyselenide Rb$_2$BaNb$_2$Se$_{11}$ is the first example for a compound in the group 1/group 2/group 5/ Q system where the structure is constructed by interconnection of the well-known Nb$_2$Se$_{11}$ building block. Compared with the hitherto known structures containing this complex unit, a new binding mode of Se^{2-}/Se$_2^{2-}$ anions with the Nb$_2$Se$_{11}$ group is observed demonstrating the flexibility and variability of the different Se^{2-} and Se$_2^{2-}$ anions. The presence of Ba^{2+} ions leads to the formation of an one-dimensional anionic chain with an interconnection of the structural building blocks never observed before. Synthetic

Fig. 3. Far-IR spectrum of Rb$_2$BaNb$_2$Se$_{11}$.

aspects as well as the chemical properties of Ba^{2+} may account for these observations. The properties of the polyselenide flux are altered in the presence of Ba^{2+} ions. Furthermore, the radius and charge of Ba^{2+} differ from those of Rb^+ yielding different local charge density and space requirements. Further explorative work is in progress to establish a transition metal chemistry with group 1/ group 2 cations. The influence of Ba^{2+} ions onto the optical properties can be observed from the change of optical band gap compared to the pure Rb compound.

References

[1] S.A. Sunshine, D. Kang, J.A. Ibers, J. Am. Chem. Soc. 109 (1987) 6202–6204.
[2] M.G. Kanatzidis, Chem. Mater. 2 (1990) 353–363.
[3] M.G. Kanatzidis, A.C. Sutorik, Prog. Inorg. Chem. 43 (1995) 151–265.
[4] W. Bensch, P. Dürichen, C. Näther, Solid State Sci. 1 (1999) 85–108.
[5] W. Bensch, C. Näther, P. Dürichen, Angew. Chem. 110 (1998) 140–142.
[6] Y.-D. Wu, C. Näther, W. Bensch, J. Solid State Chem. 178 (2005) 1569–1574.
[7] P. Dürichen, O. Krause, W. Bensch, Chem. Mater. 10 (1998) 2127–2134.
[8] P. Dürichen, M. Bolte, W. Bensch, J. Solid State Chem. 140 (1998) 97–102.
[9] O. Tougait, J.A. Ibers, Solid State Sci. 1 (1999) 523–534.
[10] Y.-J. Lu, J.A. Ibers, Inorg. Chem. 30 (1991) 3317–3320.
[11] Y.-D. Wu, C. Näther, W. Bensch, Z. Naturforsch. 59b (2004) 1006–1014.
[12] Y.-D. Wu, T.h. Doert, W. Bensch, Z. Anorg. Allg. Chem. 631 (2005) 3019–3024.
[13] Y.-D. Wu, C. Näther, N. Lehnert, W. Bensch, Solid State Sci. 7 (2005) 1062–1069.
[14] F. Hulliger, T. Siegrist, Z. Naturforsch. 36b (1981) 14–15.
[15] Bruker, SHELXTL Version 5.1, Bruker AXS Inc. Madison, Wisconsin, USA, 1998.
[16] P. Kulbelka, F. Munk, Z. Tech. Phys. 12 (1931) 593–601.
[17] C.L. Teske, N. Lehnert, W. Bensch, Z. Anorg. Allg. Chem. 628 (2002) 2651–2655.
[18] S. Schreiner, L. Aleandri, D. Kang, J.A. Ibers, Inorg. Chem. 28 (1989) 392–393.
[19] R.D. Shannon, Acta Crystallogr. A32 (1976) 751–767.
[20] T. Ikari, F. Levy, J. Phys. C: Solid State Phys. 18 (1985) L1109–L1113.
[21] P. Böttcher, J. Getzschmann, R. Keller, Z. Anorg. Allg. Chem. 619 (1993) 476–488.
[22] A. Maaninen, J. Konu, R.S. Laitinen, T. Chivers, G. Schatte, J. Pietikäinen, M. Ahlgren, Inorg. Chem. 40 (2001) 3539–3543.
[23] K.H. Schmidt, A. Müller, J. Mol. Struct. 11 (1972) 275–282.
[24] L.J. Farrugia, J. Appl. Cryst. 32 (1999) 837–838.